RSC Advances

PAPER

View Article Online
View Journal | View Issue

Cite this: *RSC Adv.*, 2020, **10**, 25652

Cell-loaded injectable gelatin/alginate/LAPONITE® nanocomposite hydrogel promotes bone healing in a critical-size rat calvarial defect model†

Bin Liu,[a] Junqin Li,[a] Xing Lei,[ab] Sheng Miao,[a] Shuaishuai Zhang,[a] Pengzhen Cheng,[a] Yue Song,[a] Hao Wu,[a] Yi Gao,[a] Long Bi*[a] and Guoxian Pei*[a]

Injectable hydrogels have long been gaining attention in the bone tissue engineering field owing to their ability to mix homogeneously with cells and therapeutic agents, minimally invasive administration, and seamless defect filling. Despite the advantages, the use of injectable hydrogels as cell delivery carriers is currently limited by the challenge of mimicking the natural microenvironment of the loaded cells, promoting cell proliferation, and enhancing bone regeneration. To overcome these problems, we aimed to develop an injectable and *in situ*-forming nanocomposite hydrogel composed of gelatin, alginate, and LAPONITE® to mimic the architecture and composition of the extracellular matrix. The encapsulated rat bone marrow mesenchymal stem cells (rBMSCs) survived in the nanocomposite hydrogel, and the gel promoted cell proliferation *in vitro*. Systematic *in vivo* research of the biomimetic hydrogel with or without cells was conducted in a critical-size (8 mm) rat bone defect model. The *in vivo* results proved that the hydrogel loaded with rBMSCs significantly promoted bone healing in rat calvarial defects, compared to the hydrogel without cells, and that the hydrogel did not provoked side effects on the recipients. Given these advantageous properties, the developed cell-loaded injectable nanocomposite hydrogel can greatly accelerate the bone healing in critical bone defects, thus providing a clinical potential candidate for orthopedic applications.

Received 4th April 2020
Accepted 30th June 2020

DOI: 10.1039/d0ra03040f

rsc.li/rsc-advances

Introduction

Injectable hydrogels have emerged over the past decade as promising biomaterials for tissue engineering applications, for example, as carriers for cell or bioactive factor delivery,[1,2] owing to their biocompatible and biodegradable nature. One of the most prominent features of hydrogels is their ability to mimic the architecture and composition of the natural extracellular matrix (ECM),[3] a complex 3D network comprised of fibrous structural proteins (*e.g.*, collagen) and polysaccharides (*e.g.* hyaluronic acid). Within this network, collagen protects the encapsulated cells from tensile and shear stress, while polysaccharides are the water-absorbing components that protects cells from compressive forces.[4,5] Benefiting from their shear-thinning behavior, hydrogels can also preserve the survival and functionalities of laden cells, by shielding high-shear forces during the injection process.[2,3] Moreover, with the rapid advance of cell-based therapies, the need to develop injectable and *in situ*-forming hydrogels as cell carriers has been growing, thus promoting the use of minimally invasive therapies in the clinic, which can reduce patient discomfort and risk of infections, and accelerate their recovery. Owing to their *in situ* gelation property, injectable hydrogels can be used to fill irregular-sized defects through minimally invasive injection, seamlessly integrating with the tissue defects and promoting *in situ* bone healing.[1,3,6]

The composition of hydrogels can be easily tailored in order to resemble that of the natural ECM and provide the necessary biochemical and biophysical cues for successful bone healing. Among the various materials studied so far, those composed of gelatin, alginate, and/or LAPONITE® have demonstrated their potential for bone tissue engineering applications.[2,3,6]

Gelatin is a product of collagen degradation, and it is a low-cost biomaterial with good cytocompatibility. As gelatin retains the Arg-Gly-Asp (RGD) sequence from the degraded collagen, it can promote cell proliferation and migration.[7] Gelatin can be gelated by thermally induced crosslinking: above 30 °C, this polymer exists in the liquid state; whereas below 30 °C, it exists as a gel.[8] To avoid dissolution at the physiological temperature (*i.e.* 37 °C), gelatin is often combined with other biomaterials to be used as an injectable hydrogel.[2] Furthermore, owing to its low mechanical strength, gelatin methacrylate (GelMA) is the most commonly used form of gelatin in bone tissue engineering.[8] However, the covalently crosslinked chemistries

[a]*Department of Orthopedics, Xijing Hospital, Fourth Military Medical University, Xi'an, 710032, P. R. China. E-mail: bilong@fmmu.edu.cn; nfperry@163.com*

[b]*Department of Orthopedics, Linyi People's Hospital, Linyi 276000, P. R. China*

† Electronic supplementary information (ESI) available. See DOI: 10.1039/d0ra03040f

generally cross-react with functional groups present on the cell surface, potentially leading to undesired effects, which may influence the survival and functionalities of laden cells.[9] In particular, production of photo-crosslinked hydrogels usually involves the use of toxic initiators that induce the generation of free radicals for the crosslinking reaction by UV or visible light exposure. Such elements—UV light, toxic initiators, and free radicals—may damage the cells.[10,11]

Alginate is an anionic polysaccharide polymer, and it is a popular biomaterial used in regenerative medicine, owing to its low cost, good biocompatibility, and convenient physical crosslinking in the presence of Ca^{2+} or Ba^{2+} *et al.*[3,12] However, alginate is a bio-inert material, as mammalian cells do not produce specific enzymes to degrade this polymer, so it is rarely used alone in bone regenerative.[13] Moreover, as mammalian cells do not produce specific enzymes to degrade it, alginate can be retained *in vivo* for a long time,[13] making it particularly suitable to use in combination with fast-degrading collagen-derived gelatin in composites. However, the lack of RGD sequences limits cell attachment and reduces its cytocompatibility. Therefore, RGD peptide modification[14] is often performed to obtain desirable cellular functions. This procedure increases the complexity and cost, and limits the application of alginate.

LAPONITE® XLG nanosilicates (LAP, $Na_{0.7}{}^{+}[(Mg_{5.5}Li_{0.3})Si_8O_{20}(OH)_4]_{0.7}{}^{-}$) is a two-dimensional (2D) synthetic nanomaterial, composed of disk-shaped nanoscale crystals with a high aspect ratio (25–30 nm in diameter and approximately 1 nm in thickness). The surfaces of the disk-shaped nanoscale crystals are negatively charged, and the edges are positively charged, thus displaying a broad-spectrum affinity with biomacromolecules.[15,16] LAP nanoplatelets are able to accelerate the gelation process through hydrogen bonds with polysaccharide matrices, such as alginate and hyaluronic acid, endowing hydrogels with superior mechanical and rheological properties, along with good injectability and self-healing ability.[3,14,16] These features make LAP able to strongly interact with anionic, cationic, and neutral polymers to form a physically crosslinked network with shear-thinning characteristics that are critical for injectable hydrogels and, thus, significantly improve their mechanical strength.[15,17] Additionally, LAP can also be used as a rheology modifier for alginate solutions.[18] Furthermore, LAP is an FDA-approved material that is generally regarded as safe, and its bioactive degradation products, such as Li^{+}, Mg^{2+} and orthosilicic acid, have been reported to promote osteogenic differentiation of human mesenchymal stem cells (hMSCs) in two-dimension (2D) culture *in vitro*.[19] In addition, when adding LAP to a GelMA solution, the generated hybrid hydrogels are capable of promoting osteogenic differentiation of MC3T3-E1 cells without the addition of growth factors.[20] However, pure LAP gels are not able to supply sufficient biochemical and biophysical cues for cell adhesion and growth. Thus, they are commonly introduced into other matrices to establish nanocomposite hydrogels. Even though previous studies have demonstrated that LAP is cytocompatible and suitable for cell culture, bone tissue engineering, and other biomedical applications, the long-term bone healing effects and possible risks associated with the use of LAP in injectable tissue engineering bone scaffolds *in vivo* are unclear and require a more thorough assessment prior to practical use.

Therefore, to mimic the natural ECM and explore a more convenient, low-cost, and biocompatible injectable hydrogel that reduces the risk of potential side effects resulting from covalent crosslinking interactions, we developed an cell-loaded injectable biomimetic nanocomposite hydrogel composed of collagen-derived gelatin, alginate, and LAPONITE® XLG for application in bone tissue engineering. In particular, we sought to take advantage of the bio-inert property of alginate to prolong the retention of the nanocomposite hydrogel *in vivo* to avoid rapid degradation by proteases[13] ensuring that the degradation rate of the hydrogel scaffold matches the rate of new bone formation. In particular, we sought to exploit the unique feature of each material: (1) the bioinert property of alginate that prolongs the retention of the nanocomposite hydrogel *in vivo* to avoid rapid degradation by proteases,[13] ensuring that the degradation rate of the hydrogel scaffold matches the rate of new bone formation; (2) the presence of the conserved RGD sequence from gelatin in alginate, known to stimulate cell proliferation and migration; and (3) the remarkable mechanical properties of LAPONITE® that provide the so-needed mechanical strength to the scaffold and the degradation elements, *e.g.*, magnesium or silicon, that enhance bone regeneration.

Experimental

Materials and methods

Materials. Gelatin (48722-500G-F) and sodium alginate (A0682-100 G) were bought from Sigma-Aldrich (St. Louis, MO, USA). LAPONITE® XLG was obtained from BYK-Chemie GmbH (Wesel, Germany).

Fabrication of the injectable nanocomposite hydrogels. Gelatin (Gel) granules, sodium alginate (Alg) powders, and LAPONITE® XLG powders were ethylene oxide-sterilized. LAP was slowly added to sterilized deionized water and mixed homogeneously using a sterilized magnetic stir rod for 60 min at room temperature. A Gel–Alg blended solution was prepared in sterilized deionized water at 40 °C. Different concentrations of pre-polymer nanocomposite hydrogel were obtained by mixing the Gel–Alg solution with the LAP solution (1 : 1); the mixture was then added to a calcium gluconate solution (0.68%) at a ratio of 1 : 1 (v/v) and homogenized. The final concentrations of the nanocomposite hydrogels are indicated in Table 1. Generally, most researchers choose 1–3% w/v LAPONITE® for the injectable hydrogels.[21–24] We choose 1%, 2% and 3% w/v

Table 1 The final concentration of the nanocomposite hydrogels

	Gelatin (w/v %)	Alginate (w/v %)	LAPONITE® XLG (w/v %)
0% LAP	5	1	0
1% LAP	5	1	1
2% LAP	5	1	2
3% LAP	5	1	3

LAP, as a gradually increasing concentration. The aim of our experiment was to evaluate the *in vitro* cytotoxicity of the additional LAPONITE® to the gelatin–alginate composite hydrogel, which has been considered nontoxic, then further to evaluate the biocompatibility of our nanoengineered injectable hydrogel and the effect of bone healing as cell carriers *in vivo*. Hence, we set LAP as the only variable in this study. As we set the concentration of LAPONITE®, from 1% w/v to 3% w/v, and according to our preliminary studies of the gelatin, alginate and LAPONITE®, the injectable shear-thinning nanocomposite hydrogel was difficult to inject through a catheter if the total solids of it exceeded 9%. Based on this, we set that the total mass of gelatin and sodium alginate is not more than 6% w/v. Previous studies of injectable hydrogels have shown that the amount of gelatin used is usually 1–10% w/v,[23,25,26] and the amount of sodium alginate used is usually 0.5–5% w/v.[27–29] Our preliminary experiments showed that the nanocomposite hydrogel (gelatin + alginate + LAPONITE®) displayed an appropriate injectability and the ability of *in situ* forming when the Gel/Alg ratio is 5 : 1. Hence, we have chosen the proportion of gelatin and alginate is 5% w/v and 1%, respectively.

Cryogenic transmission electron microscopy (Cryo-TEM). In order to acquire cryo-TEM (FEI Talos F200C, America) images of LAPONITE® XLG, 2% pure LAPONITE® XLG nanosilicate suspension was prepared with deionized water and mounted on a holey carbon copper grid (200 mesh size). Subsequently, the grid was frozen in liquid ethane and transferred to the cryo-holder for imaging at an accelerator voltage of 5 keV.

X-ray diffraction (XRD). The XRD (X'Pert Pro, Philips, Netherlands) was used to determine the phase composition of two lyophilized hydrogel samples (0% LAP and 2% LAP) and pure LAP powder. The freeze-dried samples were compressed using a pair of cover glasses to a size of 0.3 mm and introduced into the sample holder. All the samples were scanned in the range of diffraction angle $2\theta = 5–80°$ with a step size of 0.02 and a scan speed of 0.4 s. The X-ray radiation was generated from Cu-Kα source with a wavelength (λ) of 0.154 nm.

Microstructure and energy-dispersive X-ray (EDX). The morphology and elemental distribution of the hydrogels were observed using a scanning electron microscope (SEM) (S-3400; Hitachi, Tokyo, Japan) equipped with a Bruker XFlash 5030 EDX spectrometer. Hydrogel samples ($n = 3$) were frozen at −80 °C, cut with a razor blade, and lyophilized. EDX mapping was performed at an accelerator voltage of 20 keV. Next, all samples were fixed and gold-sputtered (layer thickness, 21 nm), and SEM was performed under identical conditions for all samples at an accelerator voltage of 5 keV.

Rheological analysis. Rheological tests were performed using a HAAKE rheometer (Thermo scientific, MARS 40/60, Germany) with a cone-plate geometry measuring system (25 mm diameter, 2° cone angle, 99 truncation gap). Flow rate sweeps were performed at a shear rate from 10^{-2} to 10^{2} s^{-1} at room temperature (*i.e.* 25 °C).

Hydration degree test. To evaluate the hydration degree of the hydrogels, samples ($n = 6$) were prepared and immersed in phosphate-buffered saline (PBS) for 24 h, and the wet weight (M_w) was measured. All samples were then lyophilized to obtain the dry weight (M_d). The hydration degrees of the hydrogels[20] were evaluated using the eqn (1):

$$\text{Hydration degree} = (M_w - M_d)/M_w \times 100\% \quad (1)$$

Cell isolation and encapsulation. rBMSCs were isolated from the femoral shaft of 2 week-old Sprague Dawley male rats and expanded to passage 3 in α-minimum Eagle's medium (α-MEM) supplemented with 10% v/v fetal bovine serum (FBS), 100 U ml^{-1} penicillin, and 100 mg ml^{-1} streptomycin (all from Gibco Biosciences, Dublin, Ireland) at 37 °C with 5% CO_2. When approximately 80–90% colony formation was observed, rBMSCs were trypsinized, counted, and collected for the subsequent *in vitro* and *in vivo* experiments.

Next, approximately 3×10^7 rBMSCs were harvested, suspended in 600 μl of cell culture medium and uniformly mixed with 10 ml of previously prepared 0% LAP, 1% LAP, 2% LAP, or 3% LAP nanocomposite hydrogel to obtain a final cell concentration of 3×10^6/ml. The influence of the LAP concentration on the proliferation of encapsulated rBMSCs was observed, and the most suitable hydrogel was chosen for the subsequent *in vivo* experiments.

Cell proliferation assay and live/dead staining assay. Cell proliferation was determined on days 1, 3, and 7 after cell loading using the CCK-8 assay (Dojindo, Kumamoto, Japan). At each time point, 1 ml of 10% CCK-8 solution in α-minimum Eagle's medium (α-MEM) supplemented with 10% v/v fetal bovine serum (FBS), 100 U ml^{-1} penicillin, and 100 mg ml^{-1} streptomycin was added to each sample ($n = 3$), and the samples were incubated for 4 h. Each sample was a cylinder with a diameter of 8 mm and a thickness of 2 mm, and was approximately 100 μl. After that, 300 μl of the culture medium from each sample was transferred to 3 wells of a 96-well plate; each well had a volume of 100 μl, and the absorbance at 450 nm was measured in a plate reader (Dragon Wellscan MK3, Labsystems, Bucharest, Romania).

After culturing *in vitro* for 1, 3, and 7 days, cell viability was assessed using a LIVE/DEAD™ viability/cytotoxicity assay kit (Invitrogen, Bioscience, Ireland). Briefly, the most suitable nanocomposite hydrogel samples ($n = 3$) were washed in PBS three times and then incubated in α-MEM containing 2 mM calcein AM (green fluorescence for live cells) and 4 mM ethidium homodimer-1 (red fluorescence for dead cells). Then, the samples were washed again with PBS three times, and images were captured using a laser scanning confocal microscope (Nikon A1R, Japan).

Surgical procedure. Thirty-six Sprague Dawley rats (male, 200–250 g) were purchased from the Laboratory Animal Center, Fourth Military Medical University (No. 61002000000913). All animal procedures were approved by and carried out in accordance with the standards of the Experimental Animal Ethics Committee of Fourth Military Medical University.

A critical-size (8 mm) rat calvarial defect model[30] was employed for the bone defect repair experiment, and all surgical procedures were completed under sterile conditions. The 36 rats were randomly assigned to three equally sized groups:

a blank control group without hydrogels therapy (BLK), a 2% LAP nanocomposite hydrogel without cell group (NH−), and a rBMSC-laden 2% LAP nanocomposite hydrogel group (NH + Cell). Briefly, after anesthetization by intraperitoneal injection of pentobarbital sodium (100 mg kg^{-1}), each rat's head was shaved and disinfected with iodophor. A sagittal incision of approximately 15 mm was made on the scalp, and the calvarium was exposed by blunt dissection. A defect of 8 mm in diameter was created in each animal. Then, 80 μl of the nanocomposite hydrogel with or without cells was injected into the defect, and the incision was closed with 3–0 silk sutures. In each group, six 2% LAP nanocomposite hydrogel scaffolds with or without cells were injected into the defects per time point.

To visualize new bone formation and mineralization, the polychrome sequential fluorescent labeling method was used. Two different fluorochromes, 20 mg kg^{-1} calcein and 30 ml kg^{-1} alizarin red S, were sequentially administered intraperitoneally at 14 and 4 days before euthanizing the rats at the 8 week ($n = 3$) and 12 week ($n = 3$) time points.

The injected nanocomposite hydrogels and the surrounding skull, hearts, livers, spleens, lungs, and kidneys were harvested at weeks 8, and 12 post-implantation. All samples were fixed in 4% paraformaldehyde for 2 days, and micro-computed tomography (micro-CT) and histological analyses were performed later.

Micro-CT analysis and histological evaluation. Micro-CT (ZKKS-MCT-SharpII, Zhongke Co., China) was performed at a voltage of 60 kV and an electric current of 67 mA. The voxel size after reconstruction was 25 × 25 × 25 μm. Based on the micro-CT results, 3D images were reconstructed by Materiaise's Interactive Medical Image Control System (MIMICS, Materialise Co., Belgium). The bone volume to total volume (BV/TV) ratio at weeks 8 and 12 after surgery was analyzed. Next, 50 μm-thick non-decalcified sections were prepared using an Exakt system (model 310 CP band system, Exakt, Oklahoma City, OK, USA), and the fluorescent labels were observed under a fluorescence microscope (BX53; Olympus, Japan). The mineral apposition rate (MAR) of new bone formation, which refers to the distance between the two different labels (μm d^{-1}), was calculated from the fluorescence images ($n = 3$).

The remaining non-decalcified samples, as well as the fixed hearts, livers, spleens, lungs, and kidneys, were decalcified in 10% EDTA for 4 weeks, embedded in paraffin, and sectioned. Serial cross-sections of decalcified samples underwent hematoxylin and eosin (H&E) (C0105, Beyotime, China) and Masson's trichrome staining (G1345, Solarbio® LIFE SCIENCE, China) according to the manufacturer's instructions. Then, images were acquired using a light microscope (BX53; Olympus, Japan) and a video camera (Soft Imaging System). The cross-sections were also immunohistochemically stained for Osterix. Deparaffinized cross-sections were incubated with proteinase K for antigen retrieval for 10 min, peroxidase blocking solution for 5 min, and 10% goat serum solution for 30 min. Then, the cross-sections were incubated with primary antibodies against Osterix followed by peroxidase-labeled polymer-conjugated secondary antibodies. The cross-sections were incubated with 3,30-diaminobenzidine at last for 10 min to visualize the antibody binding.

Statistical analysis. The data are presented as the mean ± standard deviation. One-way analysis of variance (ANOVA) or Student's *t*-test was used to analyze the significant differences between samples. For all tests, the level of significance was set to $*p < 0.05$, $**p < 0.01$ and $***p < 0.001$.

Results and discussion

Injectable formulations of living cells and/or bioactive molecules/drugs using hydrogels would be an ideal route of administration to the irregular target area through minimally invasive therapies. In particular, high hydration degree and proliferation are critical for cell delivery in 3D constructs. To maintain the survival and self-proliferation characteristics of the laden cells, it is critical for the biomaterials to mimic the natural ECM. Therefore, we developed and characterized a biomimetic nanocomposite hydrogel composed of Gel, Alg, and LAP to simulate the architecture and composition of ECM (Fig. 1).

Physical characterization of the nanocomposite hydrogels

Cryo-TEM images of the 2% w/v pure LAP suspension showed that the LAPONITE® were nanosheets with a diameter of 25–30 nm, which met the requirements of this experiment (Fig. 2A). The presence of LAP in the nanocomposite hydrogel was evident in the XRD spectra, in which the characteristic diffraction peaks of LAP appear in the pattern of the nanocomposite hydrogel. The XRD pattern of LAP showed the typical peaks at 35° and 61° in the spectra of both nanocomposite hydrogel (Gel + Alg + LAP) and pure LAP powder samples (Fig. 2B). EDX was performed to demonstrate the presence of silicon and magnesium in the nanocomposite hydrogel; these elements were not observed in the Gel–Alg hydrogel without LAP (Fig. 2C–D). Furthermore, SEM images confirmed no obvious particle aggregation in the nanocomposite hydrogel (Fig. 2C–D).

Rheological analysis of the injectability

To investigate the injectability and rheological characteristics of the four hydrogels (0% LAP, 1% LAP, 2% LAP, and 3% LAP), the shear-thinning behavior was examined at room temperature (*i.e.* 25 °C). Fig. 3A shows that the addition of LAP significantly

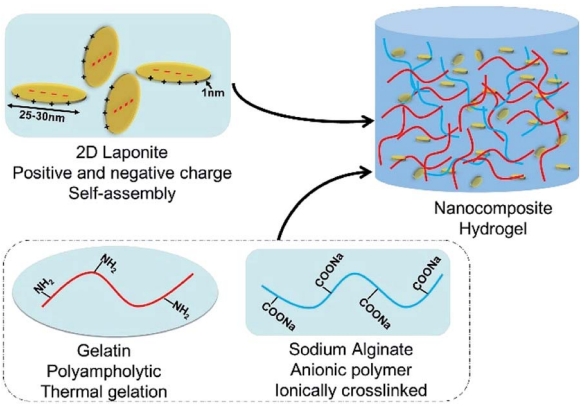

Fig. 1 Schematic of the preparation of the nanocomposite hydrogel.

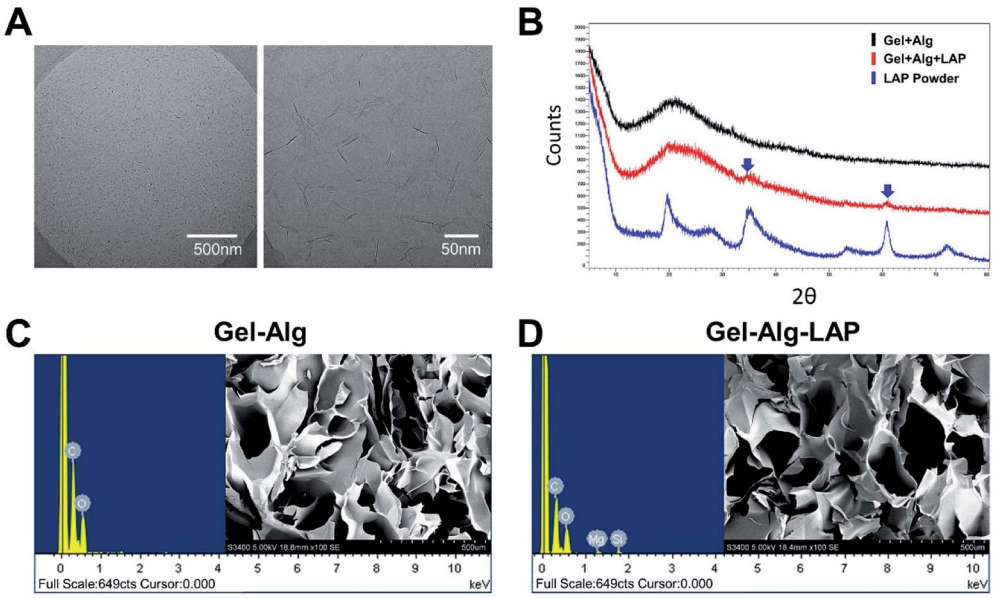

Fig. 2 Physical characterization of the nanocomposite hydrogel. (A) Cryo-TEM image of the 2% w/v pure LAP suspension. (B) XRD spectra of Gel–Alg, Gel–Alg–LAP, and pure LAP powder. (C) and (D). The results of EDX measurements of Gel–Alg composite hydrogel and Gel–Alg–LAP nanocomposite hydrogel; the SEM images suggest that the LAP nanoparticles were uniformly distributed within the polymeric network, with no nanoparticle aggregation and phase separation. (LAP, LAPONITE®; Gel, gelatin; Alg, alginate; Cryo-TEM, cryogenic transmission electron microscopy; XRD, X-ray diffraction; EDX, energy-dispersive X-ray; SEM, scanning electron microscopy).

increased the viscosity of the solutions. The four hydrogel solutions displayed a clear shear-thinning behavior, as a significant decrease in viscosity was observed with increasing shear rate. The shear-thinning characteristic can guarantee the injectability of the nanocomposite hydrogels, protect the embedded cells from damage due to shear stress, and improve the delivery efficiency of live cells.

Hydration properties of the hydrogels

The hydration degree of the hydrogels plays a critical role in determining their applicability in the biotechnological and biomedical fields. The diffusion of nutrients and waste products strongly depends on the hydration properties of the biomaterials, and is essential for the viability of laden cells.[20,31] The hydration degree of Gel–Alg-based hydrogels with different concentrations of LAP were evaluated in PBS. The hydration degree decreased with the increase of LAP concentration from 1% to 3% when compared to pure Gel–Alg hydrogel (0% LAP) (Fig. 3B). Nevertheless, the hydration degree remained greater than 90% in the case of the 2% LAP nanocomposite hydrogels, which is sufficient to maintain high cell viability. The hydration degree of the 3% LAP was lower than 90%, which may be considered unsuitable for the laden cells.

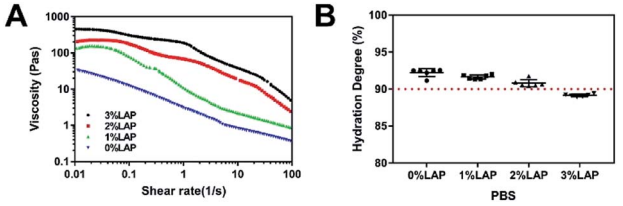

Fig. 3 Rheological analysis and hydration degree test. (A) Shear rate sweep at 25 °C illustrated the shear-thinning characteristics of hydrogels with different concentrations of LAP. (B) The hydration degree of the Gel–Alg-based hydrogels with different concentrations of LAP in PBS. (LAP, LAPONITE®; Gel, gelatin; Alg, alginate; PBS, phosphate-buffered saline).

Nanocomposite hydrogel supports cell viability and proliferation *in vitro*

The protection of the shear-thinning characteristic and the high hydration degree of the nanocomposite hydrogels guarantee the efficiency of cell delivery, and may improve the survival of laden-cells. In order to optimize the appropriate injectable formulation, we evaluated the proliferation of the encapsulated cells in four injectable formulations.

The four injectable Gel–Alg–LAP nanocomposite hydrogels (0% LAP/1% LAP/2% LAP/3% LAP) loaded with rBMSCs was biofabricated under aseptic conditions (Fig. 4).

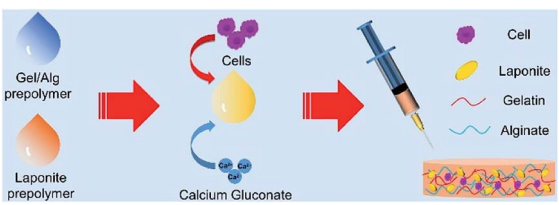

Fig. 4 Schematic of the injection process using nanocomposite hydrogels. (LAP, LAPONITE®; Gel, gelatin; Alg, alginate; PBS, phosphate-buffered saline; rBMSC, rat bone marrow mesenchymal stem cell).

Proliferation of the encapsulated cells was determined by CCK-8 assay. As shown in Fig. 5A, a continuous increase in cell proliferation was observed from day 1 to day 7 in all samples. After culturing for 1, 3, and 7 days, the proliferation of the loaded cells within 2% LAP nanocomposite hydrogel was the highest in the four hydrogels (0% LAP/1% LAP/2% LAP/3% LAP). The cells embedded in the 2% LAP nanocomposite hydrogel exhibited the most apparent proliferation ability compared with the cells within the 0% LAP, 1% LAP, and 3% LAP hydrogels. The results indicate that the laden cells maintained good viability and proliferated well, and that the additional LAP did not induce apparent toxicity to the laden rBMSCs. In addition, according to our preliminary studies of the gelatin, alginate and LAPONITE®, injectable shear-thinning nanocomposite hydrogel was difficult to inject through a catheter if the total solids of it exceeded 9%. Hence, to guarantee the proliferation of the laden cells and the injectability of the nanocomposite hydrogel, we finally chose the 2% LAP nanocomposite hydrogel as the cell delivery carrier in the subsequent experiments.

To further evaluate the survival of the laden cells, live/dead cell staining was performed for the rBMSCs laden 2% LAP hydrogels. Observations of the 3D reconstructions revealed many living cells (green color) that were uniformly distributed within the hydrogel (Fig. 5B). Since LAP and the red dye, ethidium homodimer-1, were bound by electrostatic interactions, the LAP wave-like structures within the hydrogel were stained red, consistent with the published literature.[32] The results demonstrated the good cytocompatibility of the nanocomposite hydrogel, and that the injection process was sufficiently mild to retain a high number of living cells after injection. The high cell viability was also related to the high hydration degree of the nanocomposite hydrogels, which provided an oxygenated and nutrient-rich microenvironment for the encapsulated cells.

Injectable Gel–Alg–LAP nanocomposite hydrogel loaded with rBMSCs enhances bone healing *in vivo*

Critical-size full-layer defects of the cranium were established as previously described.[30] No infection was observed during the experimental period. The time points of 8 weeks and 12 weeks were chosen in order to evaluate bone healing of the defects filled with the rBMSCs-laden 2% LAP nanocomposite hydrogel (NH + Cell group), and the 2% LAP nanocomposite hydrogel without cells (NH − group), and of the defects that did not receive hydrogel therapy (BLK group).

First, micro-CT was applied to measure the new bone mass of the defects. Fig. 6A shows representative 3D reconstruction images of the treated and non-treated defects; new bone is marked by the yellow circle (8 mm in diameter). The top view clearly shows that the NH + Cell group exhibited better bone formation than the NH − group, and that both treatment groups exhibited significantly better bone formation than the BLK group. A quantitative analysis (Fig. 6B) was performed to further evaluate the observed results. By week 8, the BV/TV ratio was 25.06 ± 0.76% in the NH + Cell group, but only 8.63 ± 0.78% in the BLK group and 14.71 ± 0.36% in the NH − group. The NH + Cell group exhibited almost 2-fold higher new bone formation than the NH − group, indicating strong promotion of bone healing in the presence of rBMSCs. By week 12, new bone occupied 32.00 ± 0.39% of the defect volume in the NH + Cell group; however, only 12.88 ± 0.53% and 20.04 ± 0.49% of the volume of the defects was filled with new bone in the BLK group and the NH − group, respectively. Combined with the 3D reconstruction observations, these results demonstrate that the promotion of bone healing and repair was greater in the NH + Cell group than in the NH − group.

Subsequently, sequential fluorescent labeling was used to observe new bone formation by applying two types of fluorochromes (Fig. 6C): calcein (green) and alizarin red (red). Because fluorochromes can bind to calcium ions of newly formed bone and be incorporated in the mineralized area, the new bone formed at different periods can be discriminated by different fluorochrome colors. Comparing the NH + Cell group with the

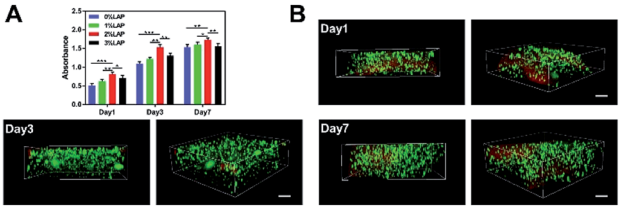

Fig. 5 The proliferation and viability of laden cells *in vitro*. (A) Proliferation of rBMSCs cultured within four different hydrogels after 1, 3, and 7 days in normal medium using the CCK-8 assay. (B) Live/dead cell staining to evaluate the cell viability after injecting the hydrogel (2% LAP). 3D reconstruction of the confocal microscope images showed numerous live cells (stained green) uniformly distributed within the nanocomposite hydrogel containing 2% LAP. LAP nanoparticles were also stained red due to electrostatic interactions with ethidium homodimer-1.[32] Scale bar: 100 μm. (LAP, LAPONITE®).

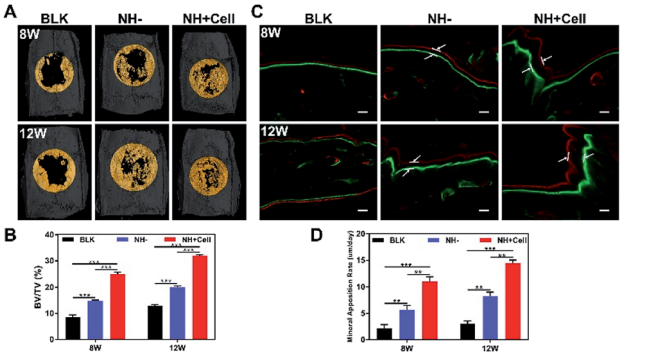

Fig. 6 Micro-CT analysis and sequential fluorescent labeling of bone healing. (A) Micro-CT 3D reconstruction of new bone formation at 8 and 12 weeks after surgery. The yellow circle is 8 mm in diameter. (B) Quantitative analysis of the BV/TV ratio of the three groups at different time points (***$p < 0.001$). (C) Representative sequential fluorescent labeling at 8 and 12 weeks after surgery for the three groups. Scale bar: 100 μm. (D) Quantitative analysis of the mineral apposition rate (μm per day) for sequential fluorescent labeling (***$p < 0.001$, **$p < 0.01$). (BV/TV, bone volume/tissue volume; BLK, blank control group without hydrogel therapy; NH−, 2% LAP nanocomposite hydrogel without cell group; NH + Cell, rBMSC-laden 2% LAP nanocomposite hydrogel group).

NH− and BLK groups, a larger interval between the two types of fluorescence signals was observed in the NH + Cell group, which indicated a faster process of new bone formation at both week 8 and week 12 post-implantation. Quantitative analysis was then performed to further evaluate the MAR. As shown in Fig. 6D, the MARs of the NH + Cell group were 11.05 ± 0.79 μm per day and 15.27 ± 061 μm per day at 8 weeks and 12 weeks post-implantation, respectively, compared with the NH− group, whose MARs were 5.65 ± 0.80 μm per day and 8.10 ± 0.64 μm per day, respectively. The MARs of the two treatment groups at 8 and 12 weeks were significantly higher than those of the BLK group (2.18 ± 0.88 μm per day and 2.09 ± 0.69 μm per day, respectively). The NH + Cell group showed the fastest MAR, which indicates the superiority of the rBMSC-laden 2% LAP nanocomposite hydrogel in terms of promotion of bone healing.

H&E staining was performed after decalcification to further evaluate new bone formation. H&E staining (Fig. 7A) showed extensive bone regeneration in the NH + Cell group at 8 weeks post-implantation. At this time point, a bony bridge began to form, while some connective tissue remained on the site of the defect. However, the defects in the BLK group were mainly filled by dense granulation tissue. Furthermore, the area of new bone formed in the NH− group was much lower than that in the NH + Cell group. At 12 weeks post-implantation, in the NH + Cell group, bony bridges appeared to connect the defect margins, and many more mature bone structures could be identified. Cortical-like lamellar bone combined with woven bone and many blood vessels appeared. In contrast, very minimal new bone formation was observed in the margin area of defects in the BLK group. The defects filled with nanocomposite hydrogel without cells exhibited cortical-like lamellar bone formation, while the new bone mass resulting from the application of this hydrogel was much lower than that resulting from the implantation of the rBMSC-laden nanocomposite hydrogel (Fig. 7B).

Masson's trichrome staining further confirmed new bone formation and maturation (Fig. 8A). In the BLK group, the defects mainly displayed blue-stained fibrous tissues. Newly formed woven bone filled larger areas in the defects of the NH + Cell group than in those of the NH− group at week 8, and the arranged bone structures exhibited cortical-like lamellar bone stained in red in the NH + Cell group. Additionally, at week 12, arranged cortical-like lamellar bone was clearly observed in the NH + Cell and the NH− groups. This was further confirmed by a quantitative analysis of the bone formation areas, showing the relative amount of new bone in the calvarial defect area from different groups (Fig. 8B).

Immunohistochemistry assessments were also performed to compare the efficacy of bone healing in different groups (Fig. S1†). For the bone-related molecule Osterix, the NH + Cell group showed significantly more expressions than the other two groups, indicating a better formation of new bone for the injectable cell-encapsulated group in the a critical-size calvarial defect. The results were coherent with the histology assessments that the NH + Cell benefited the treatment of bone defects.

To confirm the long-term biosafety of the injectable nanocomposite hydrogels, H&E staining of rat heart, liver, spleen, lung, and kidney after implantation for 12 weeks was performed. No obvious histopathological abnormalities were found in the observed organizations (Fig. 9).

In general, these *in vivo* results sufficiently demonstrate the efficient bone healing ability of the nanocomposite hydrogel loaded with rBMSCs. The combination and optimization of gelatin–alginate and LAP hold great promise for bone

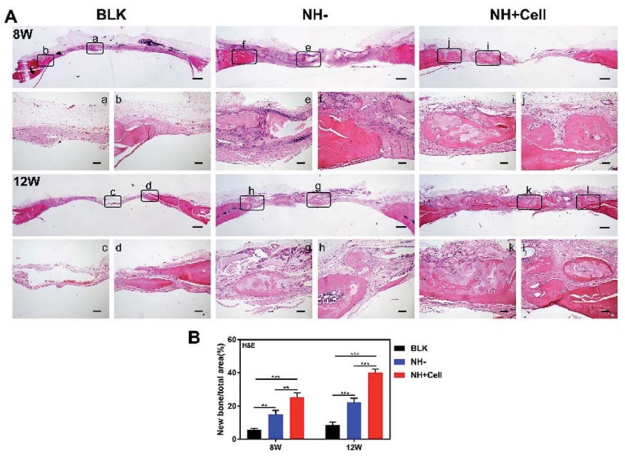

Fig. 7 H&E staining of the decalcified sections. (A) (a and c) Middle of the defect in the blank control group (BLK). (b and d) Margin of the defect in the BLK group. (e and g) Middle of the defect in the 2% LAP nanocomposite hydrogel without cell group (NH−). (f and h) Margin of the defect in the NH− group. (i and k) Middle of the defect in the rBMSCs-laden 2% LAP nanocomposite hydrogel group (NH + Cell). (j and l) Margin of the defect in the NH + Cell group. Scale bars: 500 μm and 100 μm. (B) Quantitative analysis of the bone formation areas for H&E staining (***$p < 0.001$, **$p < 0.01$).

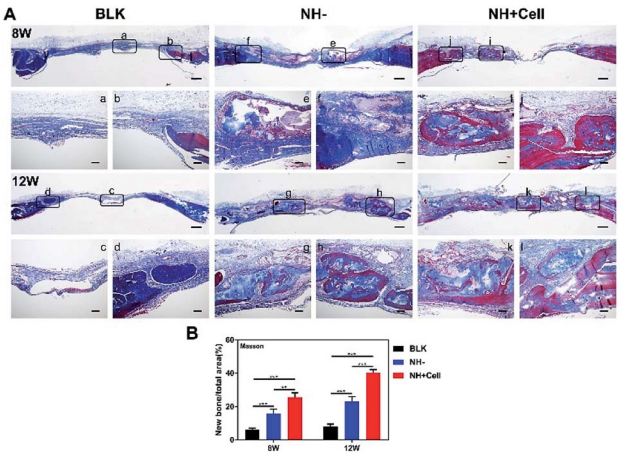

Fig. 8 Masson's trichrome staining of the decalcified sections. (A) (a and c) Middle of the defect in the blank control group (BLK). (b and d) Margin of the defect in the BLK group. (e and g) Middle of the defect in the 2% LAP nanocomposite hydrogel without cell group (NH−). (f and h) Margin of the defect in the NH− group. (i and k) Middle of the defect in the rBMSCs-laden 2% LAP nanocomposite hydrogel group (NH + Cell). (j and l) Margin of the defect in the NH + Cell group. Scale bars: 500 μm and 100 μm. (B) Quantitative analysis of the bone formation areas for Masson staining (***$p < 0.001$, **$p < 0.01$).

regeneration. The critical defect fully filled with regenerated bone within experimental time will soon be achieved. On one hand, these results may partly be due to the well-known bioactivity of the degradation products of the nanocomposite hydrogel (*e.g.*, Mg^{2+}, orthosilicic acid, and Li^{+}), which have been demonstrated to promote bone formation *in vivo*.[20,33] Additionally, our *in vivo* results also show that the defects of the NH− group exhibited excellent bone healing ability compared with those of the BLK group. On the other hand, the excellent bone repair ability may attribute to the potential osteogenesis ability of the encapsulated rBMSCs. Further experiments of ectopic bone formation should be carried out to confirm this speculation.

Moreover, recent studies have shown that the paracrine effects of mesenchymal stem cells (MSCs) in response to the local microenvironment play a critical role in injured tissue.[34,35] Among these paracrine effects, the immunomodulation ability, such as modulation of the switch of the macrophages from M1 to M2 phenotype, and the beneficial reprogramming events play particularly crucial roles in tissue engineering to promote tissue repair.[36,37] Li *et al.*[38] also showed that rBMSCs could reverse the phenotype switch of macrophages induced by LAP, inhibit proinflammatory cytokines, and promote the production of anti-inflammatory factors and osteo-related cytokines *in vitro* and *in vivo*. However, the recruitment of MSCs by the implanted scaffold *in vivo* also needs 7 days, with anti-inflammatory macrophages which could release high levels of immunomodulatory factors to bring tissue-forming MSCs to the site of damage.[39–41] So, it is important to deliver the MSCs to the damaged site of bone defects with the injectable hydrogel in the early stage of injury to accelerate the repair process of the injured tissue. Therefore, considering the osteoimmunomodulatory effects of MSCs, paracrine effects may be a mechanism underlying the progression of osteogenesis observed in the NH + Cell group. The underlying mechanism should be further studied to elucidate the strong osteoinductivity of this cell-loaded injectable nanocomposite biomaterial in our future work.

Our novel nanocomposite hydrogel system can be utilized not only as stem cells carriers for non-load-bearing injury site such as cranial defects, but also synthetic biological carriers for bioactive molecules/drugs, or currently available tissue grafts for regenerative medicine, as LAP was initially applied by several researchers in drug and/or bio-activator delivery systems. For example, Becher *et al.*[42] recently described a new drug delivery platform based on LAP nanodiscs. In our studies, we also have avoided covalent modification of gelatin and only used Ca^{2+} for crosslinking in order to retain the natural affinity toward proteins and the high activity of the nanocomposite.[43,44] Hence, our LAP nanocomposite hydrogel can be used not only as cell delivery carrier in bone tissue engineering, but can also be applied for controlled drug release or screening and for delivery of bioactive factors, such as vascular endothelial growth factor, bone morphogenetic protein-2, which expands its range of application.

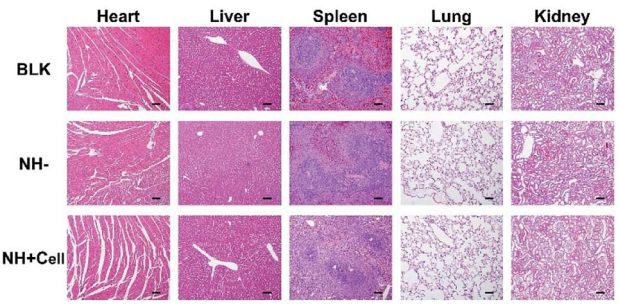

Fig. 9 H&E staining of rat heart, liver, spleen, lung, and kidney 12 weeks after implantation of the nanocomposite hydrogels with or without cells. No obvious abnormalities in the observed organizations. Scale bar: 100 μm. (BLK, blank control group without hydrogel therapy; NH−, 2% LAP nanocomposite hydrogel without cell group; NH + Cell, rBMSCs-laden 2% LAP nanocomposite hydrogel group).

Conclusions

In conclusion, we successfully developed and characterized an injectable and biomimetic nanocomposite hydrogel as cell delivery carrier to promote bone healing. The nanocomposite hydrogel was confirmed to be cytocompatible with the laden rBMSCs, and the encapsulated cells demonstrated excellent survival and proliferation. The safety of and the rapid bone healing capability promoted by the nanocomposite hydrogel loaded with rBMSCs were further demonstrated *in vivo* in a critical-size (8 mm) rat bone defect model. The results of the *in vivo* study provide evidence of the potential of this candidate material for orthopedic applications. As LAP has also demonstrated excellent drug or bioactive factors loading capacity, we expect that LAP-containing nanocomposite hydrogels could be useful for drug testing or for delivering bioactive factors to the target tissue.

Conflicts of interest

There are no conflicts to declare.

Acknowledgements

This research was funded by the National Key R&D Program of China, grant number 2016YFC1100300; and the National Natural Science Foundation of China, grant number 81672189, 81430049 and 81902202.

References

1 S. Mantha, S. Pillai, P. Khayambashi, A. Upadhyay, Y. Zhang, O. Tao, H. M. Pham and S. D. Tran, Smart Hydrogels in Tissue Engineering and Regenerative Medicine, *Materials*, 2019, **12**, 3323.
2 M. Anamizu and Y. Tabata, Design of injectable hydrogels of gelatin and alginate with ferric ions for cell transplantation, *Acta Biomater.*, 2019, **100**, 184–190.
3 A. C. Hernández-González, L. Téllez-Jurado and L. M. Rodríguez-Lorenzo, Alginate hydrogels for bone tissue engineering, from injectables to bioprinting: a review, *Carbohydr. Polym.*, 2020, **229**, 115514.

4 Y. Ma, M. Lin, G. Huang, Y. Li, S. Wang, G. Bai, T. J. Lu and F. Xu, 3D Spatiotemporal Mechanical Microenvironment: A Hydrogel-Based Platform for Guiding Stem Cell Fate, *Adv. Mater.*, 2018, **30**, e1705911.

5 G. Huang, F. Li, X. Zhao, Y. Ma, Y. Li, M. Lin, G. Jin, T. J. Lu, G. M. Genin and F. Xu, Functional and Biomimetic Materials for Engineering of the Three-Dimensional Cell Microenvironment, *Chem. Rev.*, 2017, **117**, 12764–12850.

6 S. Hou, X. Niu, L. Li, J. Zhou, Z. Qian, D. Yao, F. Yang, P. X. Ma and Y. Fan, Simultaneous nano- and microscale structural control of injectable hydrogels via the assembly of nanofibrous protein microparticles for tissue regeneration, *Biomaterials*, 2019, **223**, 119458.

7 S. Sakai, K. Hirose, K. Taguchi, Y. Ogushi and K. Kawakami, An injectable, in situ enzymatically gellable, gelatin derivative for drug delivery and tissue engineering, *Biomaterials*, 2009, **30**, 3371–3377.

8 H. Dominique and D. Madeleine, Physically and Chemically Crosslinked Gelatin Gels, *Macromol. Symp.*, 2006, **241**, 23–27.

9 C. M. Madl, L. M. Katz and S. C. Heilshorn, Bio-Orthogonally Crosslinked, Engineered Protein Hydrogels with Tunable Mechanics and Biochemistry for Cell Encapsulation, *Adv. Funct. Mater.*, 2016, **26**, 3612–3620.

10 K. Yue, G. Trujillo-de Santiago, M. M. Alvarez, A. Tamayol, N. Annabi and A. Khademhosseini, Synthesis, Properties, and Biomedical Applications of Gelatin Methacryloyl (GelMA) Hydrogels, *Biomaterials*, 2015, **73**, 254–271.

11 B. H. Lee, N. Lum, L. Y. Seow, P. Q. Lim and L. P. Tan, Synthesis and Characterization of Types A and B Gelatin Methacryloyl for Bioink Applications, *Materials*, 2016, **9**, 797–810.

12 M. Ojansivu, A. Rashad, A. Ahlinder, J. Massera, A. Mishra, K. Syverud, A. Finne-Wistrand, S. Miettinen and K. Mustafa, Wood-based nanocellulose and bioactive glass modified gelatin-alginate bioinks for 3D bioprinting of bone cells, *Biofabrication*, 2019, **11**, 035010.

13 O. Chaudhuri, L. Gu, D. Klumpers, M. Darnell, S. A. Bencherif, J. C. Weaver, N. Huebsch, H. P. Lee, E. Lippens, G. N. Duda and D. J. Mooney, Hydrogels with tunable stress relaxation regulate stem cell fate and activity, *Nat. Mater.*, 2016, **15**, 326–334.

14 K. Y. Lee and D. J. Mooney, Alginate: properties and biomedical applications, *Prog. Polym. Sci.*, 2012, **37**, 106–126.

15 A. K. Gaharwar, L. M. Cross, C. W. Peak, K. Gold, J. K. Carrow, A. Brokesh and K. A. Singh, 2D Nanoclay for Biomedical Applications: Regenerative Medicine, Therapeutic Delivery, and Additive Manufacturing, *Adv. Mater.*, 2019, **31**, e1900332.

16 S. T. Koshy, D. K. Y. Zhang, J. M. Grolman, A. G. Stafford and D. J. Mooney, Injectable nanocomposite cryogels for versatile protein drug delivery, *Acta Biomater.*, 2018, **65**, 36–43.

17 A. Sheikhi, S. Afewerki, R. Oklu, A. K. Gaharwar and A. Khademhosseini, Effect of ionic strength on shear-thinning nanoclay-polymer composite hydrogels, *Biomater. Sci.*, 2018, **6**, 2073–2083.

18 J. L. Dávila and M. A. d'Ávila, Laponite as a rheology modifier of alginate solutions: Physical gelation and aging evolution, *Carbohydr. Polym.*, 2017, **157**, 1–8.

19 A. K. Gaharwar, S. M. Mihaila, A. Swami, A. Patel, S. Sant, R. L. Reis, A. P. Marques, M. E. Gomes and A. Khademhosseini, Bioactive silicate nanoplatelets for osteogenic differentiation of human mesenchymal stem cells, *Adv. Mater.*, 2013, **25**, 3329–3336.

20 J. R. Xavier, T. Thakur, P. Desai, M. K. Jaiswal, N. Sears, E. Cosgriff-Hernandez, R. Kaunas and A. K. Gaharwar, Bioactive nanoengineered hydrogels for bone tissue engineering: a growth-factor-free approach, *ACS Nano*, 2015, **9**, 3109–3118.

21 C. Wang, Z. Gong, X. Huang, J. Wang, K. Xia, L. Ying, J. Shu, C. Yu, X. Zhou, F. Li, C. Liang and Q. Chen, An Injectable heparin-Laponite Hydrogel Bridge FGF4 for Spinal Cord Injury by Stabilizing Microtubule and Improving Mitochondrial Function, *Theranostics*, 2019, **9**, 7016–7032.

22 D. J. Page, C. E. Clarkin, R. Mani, N. A. Khan, J. I. Dawson and N. D. Evans, Injectable nanoclay gels for angiogenesis, *Acta Biomater.*, 2019, **100**, 378–387.

23 C. Xue, H. Xie, J. Eichenbaum, Y. Chen, Y. Wang, F. W. van den Dolder, J. Lee, K. Lee, S. Zhang, W. Sun, A. Amir Sheikhi, S. Ahadian, N. Ashammakhi, M. R. Dokmeci, H. J. Kim and A. Khademhosseini, Synthesis of Injectable Shear-Thinning Biomaterials of Various Compositions of Gelatin and Synthetic Silicate Nanoplatelet, *Biotechnol. J.*, 2020, e1900456.

24 G. Lokhande, J. K. Carrow, T. Thakur, J. R. Xavier, M. Parani, K. J. Bayless and A. K. Gaharwar, Nanoengineered Injectable Hydrogels for Wound Healing Application, *Acta Biomater.*, 2018, **70**, 35–47.

25 D. M. Gibbs, C. R. Black, J. I. Dawson and R. O. Oreffo, A review of hydrogel use in fracture healing and bone regeneration, *J. Tissue Eng. Regener. Med.*, 2016, **10**, 187–198.

26 M. C. Echave, R. Hernáez-Moya, L. Iturriaga, J. L. Pedraz, R. Lakshminarayanan, A. Dolatshahi-Pirouz, N. Taebnia and G. Orive, Recent advances in gelatin-based therapeutics, *Expert Opin. Biol. Ther.*, 2019, **19**, 773–779.

27 J. Venkatesan, I. Bhatnagar, P. Manivasagan, K. H. Kang and S. K. Kim, Alginate Composites for Bone Tissue Engineering: A Review, *Int. J. Biol. Macromol.*, 2015, **72**, 269–281.

28 S. Reakasame and A. R. Boccaccini, Oxidized Alginate-Based Hydrogels for Tissue Engineering Applications: A Review, *Biomacromolecules*, 2018, **19**, 3–21.

29 G. Cattelan, A. G. Gerbolés, R. Foresti, P. P. Pramstaller, A. Rossini, M. Miragoli and C. C. Malvezzi, Alginate Formulations: Current Developments in the Race for Hydrogel-Based Cardiac Regeneration, *Front. Bioeng. Biotech.*, 2020, **8**, 414.

30 P. P. Spicer, J. D. Kretlow, S. Young, J. A. Jansen, F. K. Kasper and A. G. Mikos, Evaluation of bone regeneration using the rat critical size calvarial defect, *Nat. Protoc.*, 2012, **7**, 1918–1929.

31 N. Annabi, J. W. Nichol, X. Zhong, C. Ji, S. Koshy, A. Khademhosseini and F. Dehghani, Controlling the

porosity and microarchitecture of hydrogels for tissue engineering, *Tissue Eng., Part B*, 2010, **16**, 371–383.

32 C. Boyer, L. Figueiredo, R. Pace, J. Lesoeur, T. Rouillon, C. L. Visage, J. F. Tassin, P. Weiss, J. Guicheux and G. Rethore, Laponite nanoparticle-associated silated hydroxypropylmethyl cellulose as an injectable reinforced interpenetrating network hydrogel for cartilage tissue engineering, *Acta Biomater.*, 2018, **65**, 112–122.

33 S. Bose, S. Tarafder and A. Bandyopadhyay, Effect of Chemistry on Osteogenesis and Angiogenesis Towards Bone Tissue Engineering Using 3D Printed Scaffolds, *Ann. Biomed. Eng.*, 2017, **45**, 261–272.

34 N. G. Singer and A. I. Caplan, Mesenchymal stem cells: mechanisms of inflammation, *Annu. Rev. Pathol.: Mech. Dis.*, 2011, **6**, 457–478.

35 M. Gnecchi, Z. Zhang, A. Ni and V. J. Dzau, Paracrine Mechanisms in Adult Stem Cell Signaling and Therapy, *Circ. Res.*, 2008, **103**, 1204–1219.

36 K. English, B. P. Mahon and K. J. Wood, Mesenchymal stromal cells; role in tissue repair, drug discovery and immune modulation, *Curr. Drug Delivery*, 2014, **11**, 561–571.

37 M. M. Carleton and M. V. Sefton, Injectable and degradable methacrylic acid hydrogel alters macrophage response in skeletal muscle, *Biomaterials*, 2019, **223**, 119477.

38 T. Li, Z. L. Liu, M. Xiao, Z. Z. Yang, M. Z. Peng, C. D. Li, X. J. Zhou and J. W. Wang, Impact of bone marrow mesenchymal stem cell immunomodulation on the osteogenic effects of laponite, *Stem Cell Res. Ther.*, 2018, **9**(100), 1–18.

39 Y. He, C. Mu, X. Shen, Z. Yuan, J. Liu, W. Chen, C. Lin, B. Tao, B. Liu and K. Cai, Peptide LL-37 coating on micro-structured titanium implants to facilitate bone formation in vivo via mesenchymal stem cell recruitment, *Acta Biomater.*, 2018, **80**, 412–424.

40 K. M. Hotchkiss, N. M. Clark and R. Olivares-Navarrete, Macrophage response to hydrophilic biomaterials regulates MSC recruitment and Thelper cell populations, *Biomaterials*, 2018, **182**, 202–215.

41 Z. Shao, X. Zhang, Y. Pi, X. Wang, Z. Jia, J. Zhu, L. Dai, W. Chen, L. Yin, H. Chen, C. Zhou and Y. Ao, Polycaprolactone electrospun mesh conjugated with an MSC affinity peptide for MSC homing in vivo, *Biomaterials*, 2012, **33**, 3375–3387.

42 T. B. Becher, M. C. P. Mendonça, M. A. de Farias, R. V. Portugal, M. B. de Jesus and C. Ornelas, Soft Nanohydrogels Based on Laponite Nanodiscs: A Versatile Drug Delivery Platform for Theranostics and Drug Cocktails, *ACS Appl. Mater. Interfaces*, 2018, **10**, 21891–21900.

43 X. Ding, J. Gao, Z. Wang, H. Awada and Y. Wang, A shear-thinning hydrogel that extends in vivo bioactivity of FGF2, *Biomaterials*, 2016, **111**, 80–89.

44 E. Y. Shin, J. H. Park, M. E. Shin, J. E. Song, M. Thangavelu, C. Carlomagno, A. Motta, C. Migliaresi and G. Khang, Injectable taurine-loaded alginate hydrogels for retinal pigment epithelium (RPE) regeneration, *Mater. Sci. Eng., C*, 2019, **103**, 109787.